molecules

MDPI

Article

One-Pot Synthesis and Evaluation of Antioxidative Stress and Anticancer Properties of an Active Chromone Derivative

Chirattikan Maicheen [1], Chokchaloemwat Churnthammakarn [2], Nichapat Pongsroypech [2], Thitiphong Khamkhenshorngphanuch [2,3], Jiraporn Ungwitayatorn [4], Kanin Rungsardthong [2], Rathapon Asasutjarit [2,3] and Sewan Theeramunkong [2,3,*]

1 Department of Pharmaceutical Chemistry, Faculty of Pharmaceutical Sciences, Huachiew Chalermprakiet University, Samut Prakan 10540, Thailand
2 Faculty of Pharmacy, Thammasat University, Pathumthani 12120, Thailand
3 Thammasat University Research Unit in Drug, Health Product Development and Application (DHP-DA), Department of Pharmaceutical Sciences, Faculty of Pharmacy, Thammasat University, Pathumthani 12120, Thailand
4 Department of Pharmaceutical Chemistry, Faculty of Pharmacy, Mahidol University, Bangkok 10400, Thailand
* Correspondence: sewan@tu.ac.th

Abstract: Chromones are the structural building blocks of several natural flavonoids. The synthesis of chromones, which contain a hydroxy group on the ring, presents some challenges. We used the one-pot method to synthesize ten chromone derivatives and two related compounds using modified Baker-Venkataraman reactions. The structures were confirmed using FT-IR, ^{1}H NMR, ^{13}C NMR, and HRMS. The in vitro antioxidant assay revealed that compounds **2e**, **2f**, **2j**, and **3i** had potent antioxidant activity and that all these synthesized compounds, except those containing nitro groups, were harmless to normal cells. In addition, compounds **2b**, **2d**, **2e**, **2f**, **2g**, **2i**, and **2j** had anticancer activity. Compounds **2f** and **2j** were used to investigate the mechanism of anticancer activity. Both **2f** and **2j** induced a slightly early apoptotic effect but significantly impacted the S phase in the cell cycle. The effect on cell invasion indicates that both compounds significantly inhibited the growth of cervical cancer cells. A chromone scaffold possesses effective chemoprotective and antioxidant properties, making it a promising candidate for antioxidant and future cancer treatments.

Keywords: chromone derivatives; anticancer; antioxidant; synthesis; quercetin

check for updates

Citation: Maicheen, C.; Churnthammakarn, C.; Pongsroypech, N.; Khamkhenshorngphanuch, T.; Ungwitayatorn, J.; Rungsardthong, K.; Asasutjarit, R.; Theeramunkong, S. One-Pot Synthesis and Evaluation of Antioxidative Stress and Anticancer Properties of an Active Chromone Derivative. *Molecules* **2023**, *28*, 3129. https://doi.org/10.3390/molecules28073129

Academic Editor: Letizia Giampietro

Received: 3 March 2023
Revised: 28 March 2023
Accepted: 30 March 2023
Published: 31 March 2023

Copyright: © 2023 by the authors. Licensee MDPI, Basel, Switzerland. This article is an open access article distributed under the terms and conditions of the Creative Commons Attribution (CC BY) license (https://creativecommons.org/licenses/by/4.0/).

1. Introduction

Generally, human bodies produce damaging substances known as free radicals, which may also play a role in redox signaling and in regulating processes involving the maintenance of homeostasis when present in low-to-moderate concentrations [1]. When there is an excess of free radicals in the body, oxidative stress occurs and contributes to the development of various chronic and metabolic disorders or cancers [2]. If not neutralized, free radicals will initiate a chain reaction that can (a) cause structural modifications to cellular proteins, (b) stop the function of critical enzymes, cellular activities, and normal cell division, (c) degrade DNA, and (d) inhibit energy production [3–7]. In addition, the fact that free radicals are associated with aging implicates the gradual accumulation of oxidative cellular damage as a fundamental driver of cellular aging [8]. Furthermore, oxidative stress stimulates the immune response, causing allergic diseases and the expression of proinflammatory genes [9,10]. Several cancers are believed to result from interactions between free radicals and DNA, resulting in mutations that alter the cell cycle and cause neoplasia [11]. Healthy organisms resist the harmful effect of reactive oxygen species (ROS) due to the balance between oxidants and antioxidants [12,13]. Since tumor cells express fewer antioxidants than normal cells, their ROS levels are higher. Moreover, tumor cells

with impaired mitochondrial oxidative metabolism exhibit elevated levels of ROS [14], making ROS induction a promising cancer strategy [15].

The antioxidant mechanism normally eliminates free radicals. Various endogenous and exogenous antioxidants protect against oxidative damage and chronic diseases [3]. Antioxidants can counteract free radicals by interfering with any of the three main stages of the oxidative process that are mediated by free radicals: initiation, propagation, and termination [16]. Flavonoids are an essential component in numerous nutraceutical, pharmaceutical, medicinal, and cosmetic applications. They have antioxidative, anti-inflammatory, antimutagenic, and anticarcinogenic properties as well as the ability to modulate key cellular enzyme functions [17,18], antifungal, antimicrobial [19], anti-parasitic properties [20]. Furthermore, flavonoids have potent inhibitory effects on several enzymes, including cyclo-oxygenase (COX), lipoxygenase, and phosphoinositide 3-kinase [17]. The flavone structure—also known as a phenyl-substituted chromone—has phenylbenzopyrone structures (C6-C3-C6) and is classified according to the saturation level and opening of the central pyran ring into flavones, flavanols, isoflavones, flavonols, flavanones and flavanonols (Figure 1) [21,22]. Notably, polyphenols have been reported to have anticarcinogenic properties against different cancers [23].

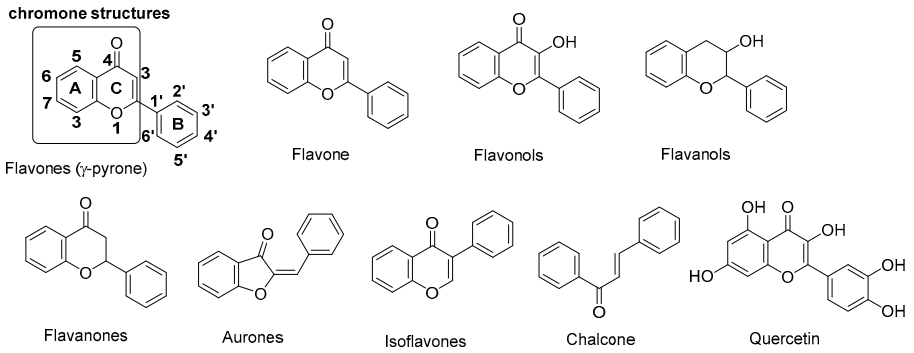


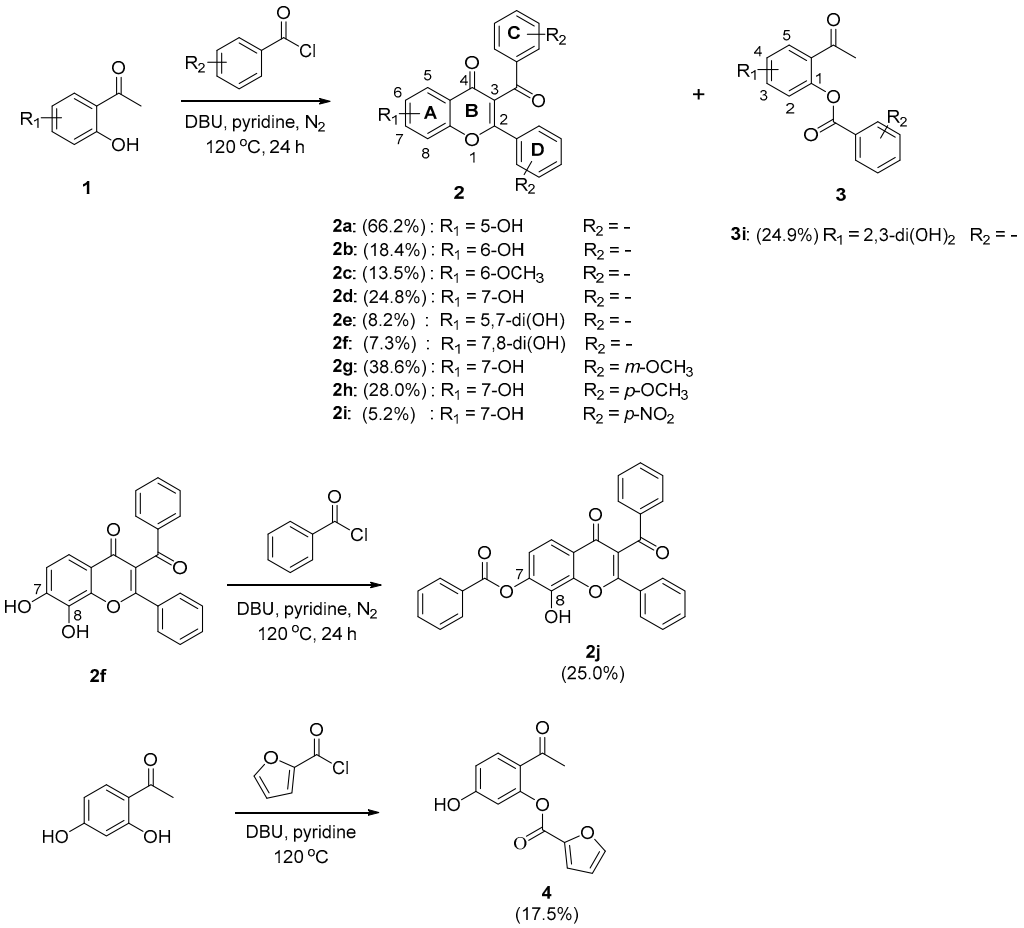
Figure 1. Structures and numbering system of flavones and derivatives.

This study aimed to design novel compounds that enhance antioxidative activity and have the chemopreventive ability to prevent or reduce cervical cancer. The designed compounds—with chromones in the core structure (**2a**–**2j**, **3i**, and **4**)—were synthesized and tested for their antioxidative capacity compared to quercetin. Using modified Baker–Venkataraman reactions, a γ-pyrone structure was synthesized in a single pot. Acetophenones **1** was heated with a suitable acyl chloride in the presence of 1,8-diazabicyclo [5.4.0]undec-7-ene (DBU) in dry pyridine to produce the corresponding chromone derivative **2** and phenolic esters **3** in low yield, as shown in previous protocol (Scheme 1) [24–26].

Our designed chromone compounds (**2a**–**2j**, **3i**, and **4**) were evaluated for their antioxidative capacity compared to the known antioxidative substance quercetin (Scheme 1). The impacts of the hydroxyl group in relation to **2a**–**2f** were investigated, as well as variations in the hydroxyl group's position in the A-ring and substituted withdrawing or donating groups that were visible in the C- and D-rings in **2g**–**2f**. In addition, the activity of the open B-ring was observed in relation to the significance of the chromone ring (**3**, **4**). At position 7, an ester substituent (**2i**) was also considered.

Three in vitro antioxidant assays (DPPH, FRAP, and ABTS) were utilized to evaluate the antioxidant property of the synthesized compounds. The DPPH (α, α-diphenyl-β-picrylhydrazyl) assay is the well-known approach to determine antioxidant activity using a stable free radical DPPH, measure the absorbance change, and calculate the absorbance change in the percentage of scavenging activity. For the FRAP (ferric reducing ability of plasma or ferric ion reducing antioxidant power) assay, this method does not involve radical generation or the scavenging of added radicals but uses a simple redox reaction. For example, the ferric-tripyridyltriazine (Fe^{3+}-TPTZ, colorless) complex is reduced to ferrous tripyridyltriazine (Fe^{2+}-TPTZ) at low pH and introduces a blue color with maximum

absorption at 593 nm. The change in absorbance is related to antioxidant activity [27,28]. However, a significant limitation of these in vitro tests is the non-physiological measurement conditions (no enzymatic condition and no transition metal ion chelating activity); therefore, the results obtained may not reflect the antioxidant activity of the source material under the biological conditions that exist in humans and animals [29,30]. The ABTS assay involves a more drastic radical that is chemically produced. The use of ABTS for antioxidant activity determination of hydrophilic and lipophilic pure compounds has attracted interest due to its solubility in organic and aqueous media and stability in a wide pH range [31].



Scheme 1. Synthesis of chromone derivatives. The reaction was carried out with acetophenone (1.0 eq), acyl chloride (2.5 eq) and DBU (3.0 eq) in dry pyridine under N_2 gas. The reaction was stirred and refluxed at 120 °C for 24 h. The crude product was purified with silica column chromatography.

Furthermore, the cytotoxicity of the synthesized compounds was examined against both normal cells (HEK293 and HACAT cells) and cervical cancer cell lines (HeLa cell). Non-toxic and active compounds were chosen to further determine the protective activity against H_2O_2-induced cytotoxicity, then verify the outcome using a cellular ROS investigation. Cellular ROS in the cell was analyzed using probes that react with ROS to compete with antioxidants and produce a stable metabolite. Finally, anti-migration and apoptosis were also studied.

2. Results and Discussion

2.1. Synthesis

The desired acetophenone (1 eq) was reacted with acyl chloride (2.5 eq) in dry pyridine using DBU (3 eq) as the base. The chromone ring was produced at a high temperature (120–140 °C) for at least 24 h. The proposed mechanism of this reaction was illustrated in Figure 2. The reaction is firstly through hydroxy of phenyl reacting to acyl chloride and

resulting non-chromone products occurred in some reactions. The crude product from synthesis was then purified by column chromatography. The product yield was obtained in the range of 5.2–66.2% (**2a**–**2j**), 24.9% (**3i**), and 17.5% (**4**). The lowest yield of the final product **2i** (5.2%) was due to the steric structure of the *nitro*- group, leading to the hindering of ring cyclization; additionally, the low yield of **2f** (7.3%) was possibly from the dihydroxy on the ring donate electron into the ring-affected C=O on the less reactive acetyl group and finally leading to low yield of the chromone ring. The synthesis protocol of **2j**, however, was the same as that of **2f,** except that 7,8-dihydroxy of the chromone ring can continue the reaction at 7-OH to form an ester group with a yield of 25.0%. During the reactions, the side products were compounds **3i** and **4**.

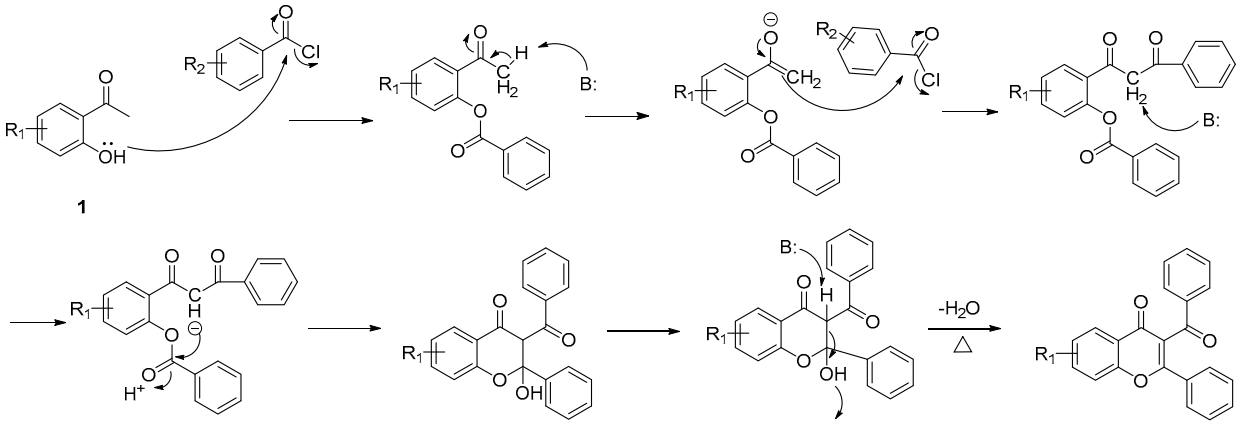


Figure 2. Purposed mechanism of chromone synthesis using modified Baker–Venkataraman reactions.

2.2. Antioxidant Activity

The in vitro antioxidant activity of the synthesized compounds was evaluated using the DPPH, FRAP, and ABTS assays. All techniques were modified and performed on 96-well plates. In addition, blank and quercetin were also performed, and the results are shown in Table 1.

Table 1. The percentage of antioxidant activity using the DPPH, FRAP, and ABTS method.

Entry	$DPPH_{517nm}$		$FRAP_{593nm}$ Value ± SD (TE, μM Trolox/1 μM of Synthesized Compounds)	$ABTS_{734nm}$	
	% SA ± SD at 10 mg/mL	EC_{50} ± SD (μM)		% Scavenging at 500 μM	EC_{50} ± SD (μM)
2a	2.23 ± 1.99	-	0.02 ± 0.004	10.93 ± 1.44	-
2b	5.32 ± 2.43	-	0.02 ± 0.003	35.99 ± 1.32	-
2c	5.88 ± 2.65	-	0.07 ± 0.028	13.16 ± 0.78	-
2d	15.85 ± 4.61	>750	0.02 ± 0.003	27.59 ± 2.46	-
2e	46.30 ± 3.61	>750	0.02 ± 0.002	80.67 ± 0.30	158.27 ± 10.87
2f	93.55 ± 3.20	34.06 ± 3.28	1.70 ± 0.138	81.63 ± 1.80	10.15 ± 0.70
2g	18.32 ± 0.40	-	0.02 ± 0.008	11.52 ± 3.56	-
2h	12.57 ± 6.18	-	0.06 ± 0.024	6.55 ± 4.19	-
2i	13.75 ± 3.31	-	0.08 ± 0.006	8.52 ± 3.89	-
2j	92.88 ± 0.46	49.91 ± 10.99	0.34 ± 0.078	>95	22.18 ± 0.39
3i	90.55 ± 0.36	58.98 ± 11.20	3.16 ± 0.350	78.80 ± 1.14	13.89 ± 0.74
4	0.99 ± 0.71	-	0.00 ± 0.001	14.51 ± 1.94	-
Quercetin	93.89 ± 2.04	18.29 ± 5.62	3.35 ± 0.231	88.51 ± 0.80	11.41 ± 0.17

Note: [a] Mean values of three measurements ± SD; SA = Scavenging activity.

2f, **2j,** and **3i** contained high in vitro antioxidant activity among these synthesized compounds. Without a chromone scaffold, compound **3i** still had high antioxidant activity. Noticeably, one part of the compound **3i** structure is similar to a simple structure of the natural protocatechuic acid (PCA), a well-known antioxidant.

2.3. Cytotoxicity Assay

Cell viability of cells treated with synthesized compounds was expressed as a percentage relative to untreated control cells (Table 2). Quercetin was used as a reference agent, which has been reported for its inhibitory activity against cervical cancer cells [32].

Table 2. The percentage of viability HEK293 cell and HACAT cell affected by synthesized compounds at 100 μM.

	% Viability ± SD (at 100 μM)			
	HEK293		HACAT	
Entry	**24 h**	**48 h**	**24 h**	**48 h**
2a	110.88 ± 6.37	102.57 ± 6.05	63.80 ± 3.36	88.54 ± 6.86
2b	105.16 ± 2.70	72.41 ± 8.55	75.71 ± 3.38	74.93 ± 1.55
2c	72.48 ± 6.46	74.03 ± 1.32	62.26 ± 3.04	60.42 ± 0.73
2d	88.65 ± 1.33	87.84 ± 1.80	77.76 ± 6.93	72.51 ± 3.41
2e	99.73 ± 2.41	93.93 ± 5.34	79.70 ± 3.26	69.11 ± 3.07
2f	105.39 ± 1.19	74.68 ± 0.83	81.60 ± 8.46	77.07 ± 5.03
2g	79.07 ± 0.90	76.74 ± 1.16	81.55 ± 5.17	78.39 ± 5.44
2h	77.24 ± 1.93	73.10 ± 0.79	75.16 ± 7.39	71.76 ± 3.27
2i	65.14 ± 1.21	41.16 ± 2.11	59.76 ± 5.77	27.51 ± 1.24
2j	96.02 ± 2.62	71.60 ± 5.19	72.58 ± 5.53	58.03 ± 2.63
3i	110.06 ± 1.20	107.23 ± 4.18	104.81 ± 0.88	84.87 ± 3.05
4	97.99 ± 0.40	108.38 ± 2.84	85.70 ± 5.60	72.17 ± 1.81
Quercetin	102.45 ± 1.58	86.62 ± 4.66	85.57 ± 125	76.82 ± 2.32

Values are mean ± SD from at least 3 separate experiments.

The results showed that most compounds were quite nontoxic in HEK293 cells, except compound **2i,** which contained *p*-NO_2 and is likely to be more toxic after 24 and 48 h treatment. This is because the nitro group on the compound has a structural alert, which is extensively associated with toxicity. Furthermore, the synthesized compounds were generally more toxic in HACAT cells than in HEK293. The anticancer activity of these compounds on cervical cancer cells was also investigated for 24 h. Compounds **2b**, **2d**, **2e**, **2f**, **2g**, **2i**, and **2j** contained anticancer activity, and four compounds (**2i, 2b**, **2j**, **2e**) had the most potent anticancer activity with the IC_{50} values 34.9, 95.7, 101.0, and 107.6 μM, respectively (Table 3). Although the anticancer activity against HeLa cells of synthetic compounds seems to be weak compared to available anticancer agents, this scaffold has potential to be a preventive treatment for humans in the future.

Table 3. The anticancer activity of synthesized compounds against HeLa cell.

Entry	% Viability ± SD (at 100 μM)		IC_{50} (μM, at 24 h)
	24 h	**48 h**	
2a	91.89 ± 2.06	58.75 ± 2.02	ND
2b	40.90± 0.41	24.82 ± 1.05	95.69 ± 1.16
2c	60.67 ± 0.57	82.12 ± 0.11	ND
2d	85.17 ± 0.79	42.36 ± 0.09	166.94 ± 0.49
2e	75.95 ± 1.52	26.46 ± 1.13	107.60 ± 4.04
2f	109.27 ± 0.92	29.16 ± 0.40	190.90 ± 6.01
2g	47.98. ± 3.10	46.28 ± 1.14	172.73 ± 1.66
2h	84.86± 2.55	64.25 ± 0.76	ND
2i	38.71 ± 5.22	12.51 ± 1.45	34.93 ± 2.41
2j	65.15 ± 1.42	30.01 ± 1.23	101.00 ± 3.18
3i	99.88 ± 4.19	37.13 ± 1.96	ND
4	86.14 ± 3.24	91.07 ± 0.65	ND
Quercetin	69.13 ± 1.93	19.21 ± 0.25	192.43 ± 1.27

The IC_{50} values represent the calculated IC_{50} values for the compounds in which a total concentration-response curve was performed. Values are mean ± SD from at least 3 separate experiments. IC_{50} values were determined only for the compounds with IC_{50} < 200 μM.

2.4. Antioxidant Activity against H_2O_2-Induced Cytotoxicity

The synthesized compounds were examined for the ability of the compounds to protect cells exposed to oxidative stress. Six active compounds from the antioxidant test, **2b**, **2d**, **2e**, **2f**, **2j**, and **3i**, were selected to study the ability of oxidative stress protection. The HEK293 cells were treated with 7.5 mM hydrogen peroxide for 30 min; samples and quercetin were added, and cell viability was investigated at 12 and 24 h treatment. The percentage of viable cells in each sample was calculated using the untreated cell as 100% survival (Figure 3).

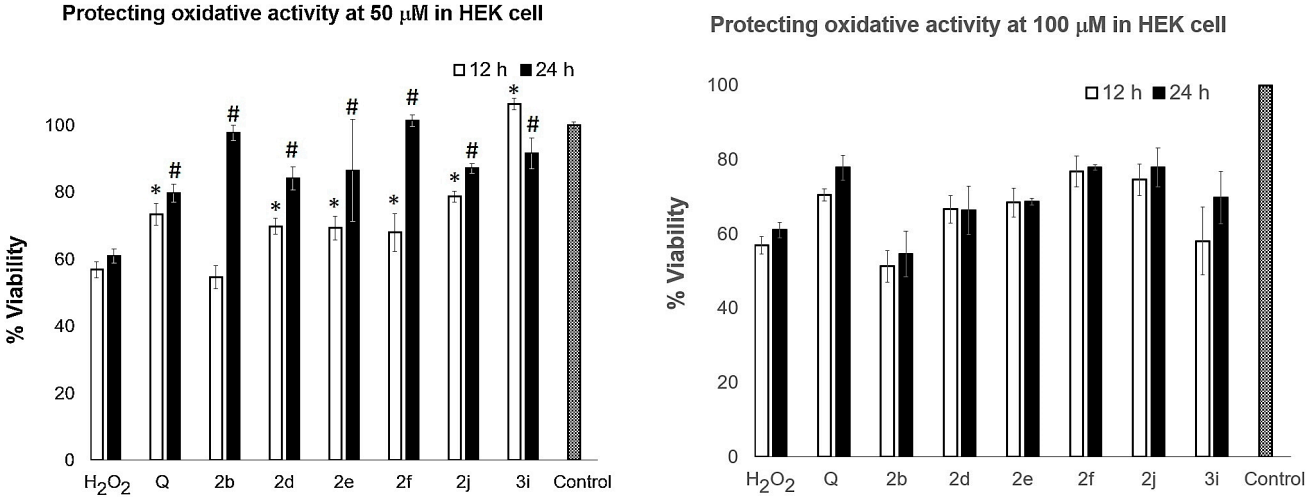


Figure 3. Protective effect of synthesized compounds on H_2O_2-induced cytotoxicity in cultured HEK cells (means ± SD, n = 3). Data (cell viability, measured by the MTT assay) were expressed as a percentage of the control group, which is 100%. The results were calculated from three independent experiments and are shown as mean ± SD. Compared to the H_2O_2 model group, the p values were calculated using a one-way ANOVA with Tukey (Turkey HSD) multiple comparison analysis; * $p < 0.05$ at 12 h treatment, # $p < 0.05$ at 24 h treatment.

Almost all compounds with 50 μM were able to significantly protect cells from oxidative stress at 24 h treatment (Figure 3). In particular, **2f** and **2j** at 100 μM were still able to protect cells from oxidative stress. Therefore, both compounds **2f** and **2j** have the potential for further investigation concerning in-cell ROS.

2.5. Cellular ROS Assay

ROS is the main contributor to cell death. These reactive molecules are formed by several mechanisms and can be detected by various techniques. In order to investigate the level of cellular ROS after treatment with compounds, the accumulation of intracellular ROS in cells was quantified with a cellular ROS assay kit (ab186029, Abcam, Boston, USA) fluorescence assay. After pretreatment with **2f**, **2j**, and **3i** at 50, 100, and 150 μM for 24 h, cell stress was induced with 5 mM hydrogen peroxide for 30 min. The cells in each well were collected and resuspended with a serum-free medium containing the ROS red probe. Subsequently, cells were incubated at 37 °C for 30 min in the dark, and fluorescence was read at Ex/Em = 650/675 nm. The fluorescence intensity of the cell after preincubation with **2f** and **2j** at 50, 100, and 150 μM was significantly reduced compared to the H_2O_2-treated cells (Figure 4). The fluorescence decreased significantly after pretreatment with **2f**, **2j,** and **3i,** and most of the fluorescence changes were among those with concentrations of 150 μM. Overall, these results suggested that pretreatment with **2f** and **2j** could reduce oxidative stress.

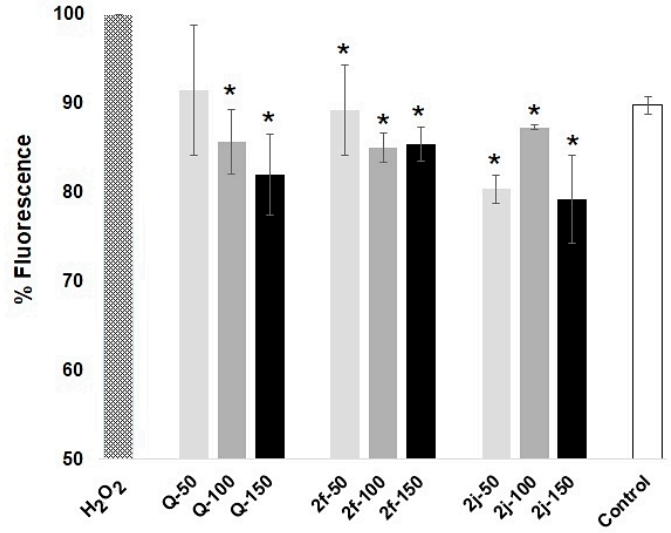


Figure 4. Fluorescence intensity of the ROS assay kit of **2f**, **2j**, and quercetin (50, 100, and 150 µM) in HeLa cells (means ± SD, $n = 3$). Data are presented as the mean ± SD for at least three independent experiments. Asterisks (*) indicate a significant difference ($p < 0.05$) compared to the H_2O_2 model group.

2.6. Apoptosis

Examining apoptosis induction by some samples was confirmed by the determination of annexin V ($p \leq 0.05$) using the IC_{50} for **2b**, **2e**, **2f**, **2j**, and quercetin in the HeLa cell line (Figure 5a). In the apoptosis profile, the cells treated with **2f** were significantly changed ($p < 0.05$) compared to the control; −12.1% in the live phase, +6.3% in the early apoptosis phase, +1.2% in the late apoptosis phase, and +5.8% in the dead phase after 24 h treatment. However, other compounds had a lower effect on apoptosis than **2f**. The results of total apoptosis are presented in Figure 5b. The results reveal that compound **2f** induced apoptosis in tumor cells, and the mechanism that mediates the cytotoxicity of this compound was apoptosis induction.

2.7. Cell Cycle Analysis

In order to understand the influence of derivatives and quercetin on the cell cycle, HeLa cells were treated with **2f** and **2j** and quercetin at the IC_{50} for 24 h and analyzed by flow cytometry (Guava Muse Cell Analyzer, Luminex, USA) with Guava suite software 3.4. The results show S phase arrest in cell cycle after treatment with concentration at IC_{50} of quercetin and **2f**, **2j** for 24 h. The pattern of cell population in the G0/G1 and S phase of quercetin and **2f**, **2j** changed dramatically from the control (Figure 6). The paclitaxel (5 µM) was performed as the positive control. The pattern of the paclitaxel cell population was evident as an active inhibitor with potent phase arrest of G2/M. The percentage of cells in phase S was 13.79%, which clearly increased to 37.88%, 34.03%, and 31.61% in quercetin, **2f**, and **2j**, respectively (Table 4). This signifies that **2f** and **2j** arrested the cells in phase S to the same degree as quercetin.

2.8. Cell Migration Assay

Cell migration in **2f** and **2j** compared to the untreated control were examined for 24 and 48 h. Quercetin was also investigated. In HEK293 cells, the migration of treated cells by **2f**, **2j**, and quercetin showed significant induction of cell migration compared to the untreated (Figure 7).

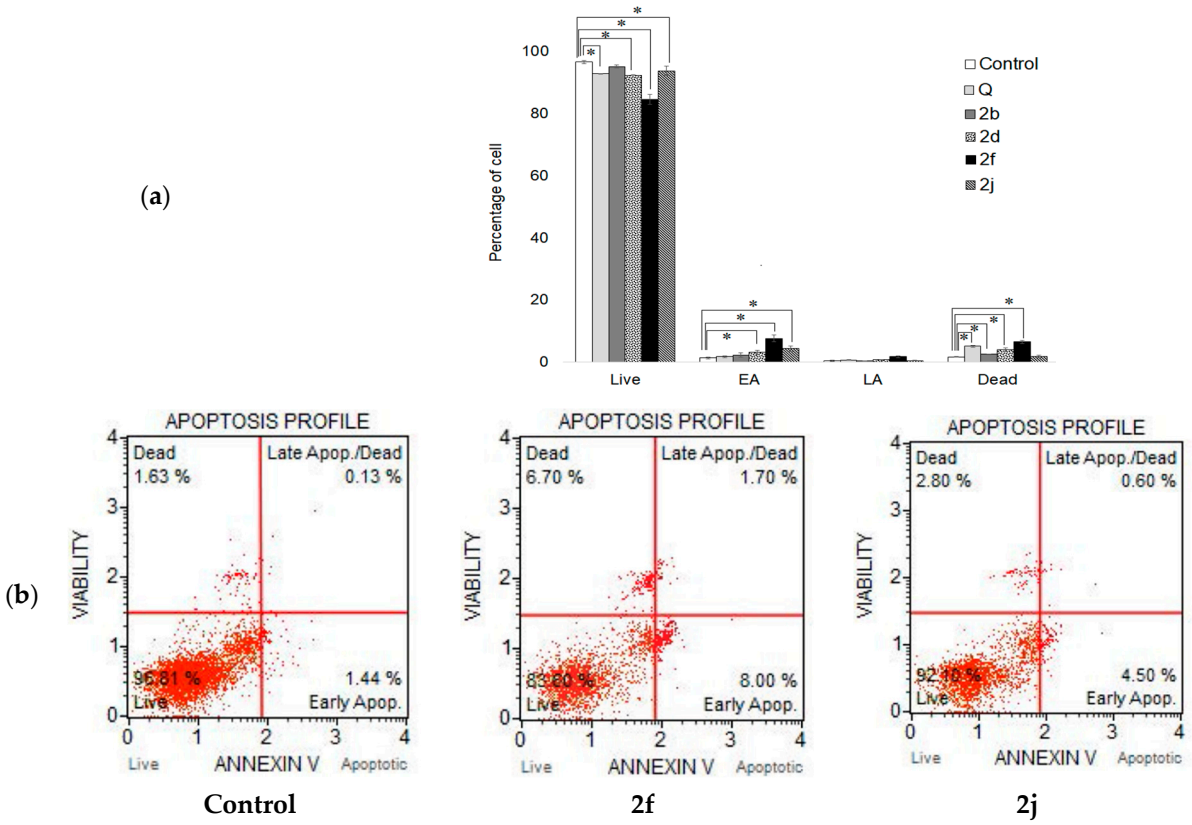


Figure 5. Cells were treated with control (medium) and samples with IC_{50}: quercetin, **2b**, **2d**, **2f**, and **2j**. The bars represent the ratios of the apoptotic cells in each group. Data from each cell cycle phase are expressed as means ± SD deviation of three independent experiments. * $p < 0.05$ vs. control group for each phase. The p values were calculated using a one-way ANOVA with Tukey's HSD multiple comparison post hoc analysis (**a**). The apoptotic effect of synthesized compounds, **2f** and **2j,** incubated for 24 h in HeLa cells (**b**).

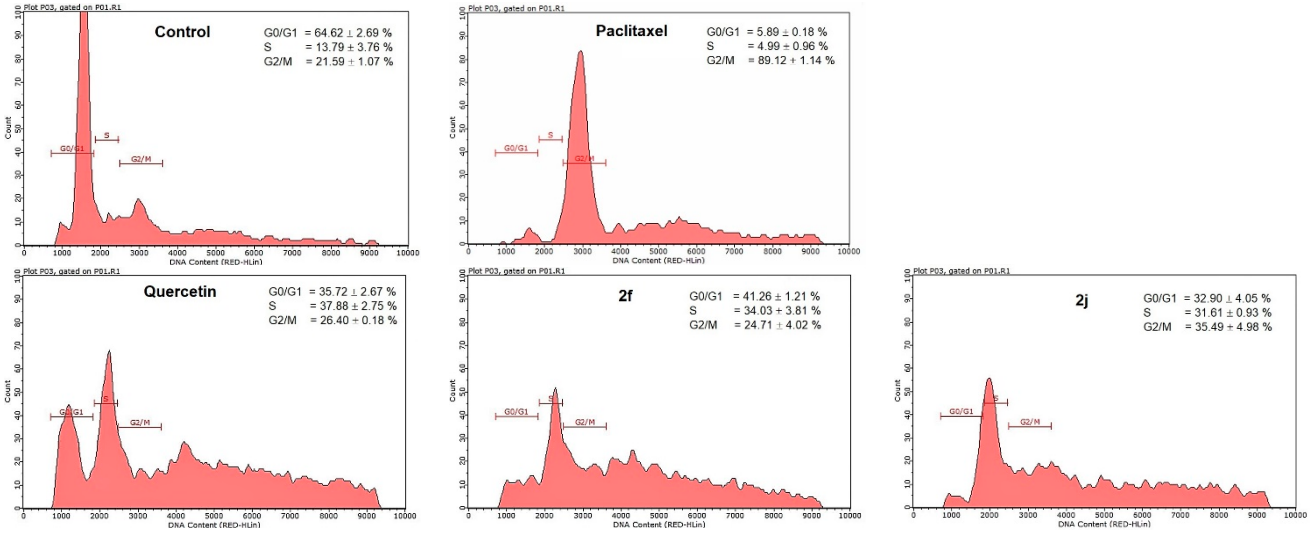


Figure 6. Flow cytometry analysis of cell cycle. Representative flow cytometry histograms of the percentage of cells in G0/G1, S, and G2/M phases of the cell cycle in HeLa cells. Cells treated with **2f**, **2j**, quercetin with concentration at IC_{50}, paclitaxel (5 μM), or untreated control for 24 h. Control and treated cells were fixed, stained, and analyzed by flow cytometry as per the Muse® cell cycle kit protocol.

Table 4. Percentage of population in each cell cycle phase after treatment with quercetin, **2f**, and **2j** in HeLa cells.

Compounds	G0/G1 (%)	S (%)	G2/M (%)
Paclitaxel	5.89 ± 0.18	4.99 ± 0.96	89.12 ± 1.14 *
Quercetin	35.72 ± 2.67	37.88 ± 2.75 *	26.40 ± 0.18
2f	41.26 ± 1.21	34.03 ± 3.81 *	24.71 ± 4.02
2j	32.90 ± 4.05	31.61 ± 0.93 *	35.49 ± 4.98
Untreated control	64.62 ± 2.69	13.79 ± 3.76	21.59 ± 1.07

* = phase in cell cycle which was significantly affected by treated compounds ($p < 0.05$).

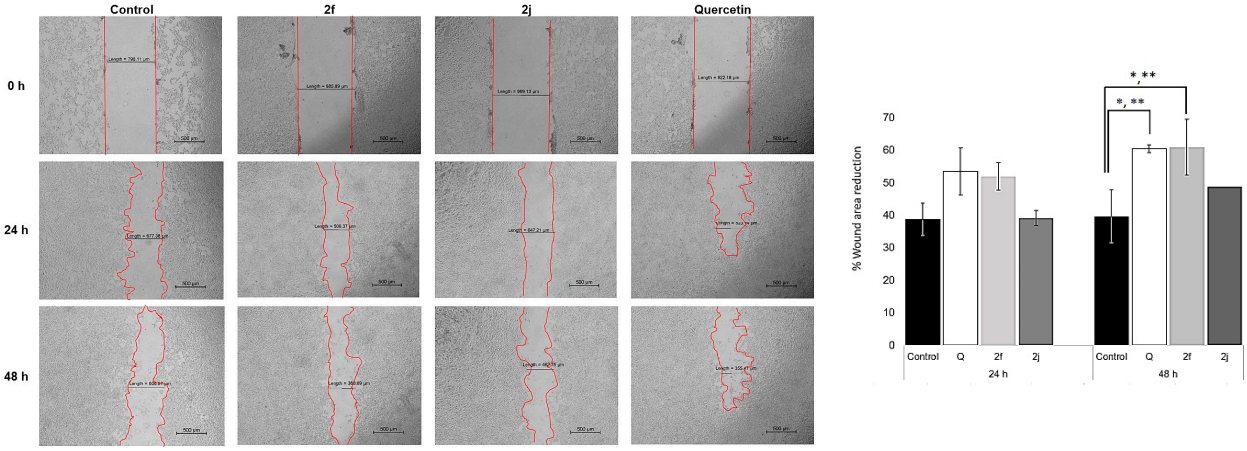


Figure 7. A scratch assay was performed to examine the migration ability of synthesized compounds **2f** and **2j** at 100 µM compared with untreated control. Representative pictures of the assay induce the migration of HEK cells using quercetin as a reference. Pictures were taken at the start of the experiment (0 h) 24 and 48 h later. Pictures of representative experiments are shown, and the relative migration of cells is represented with a bar graph; means ± SD ($n = 3$; *: $p < 0.05$ and **: $p < 0.001$, Turkey HSD), Scale bars represent 500 µm.

In addition, the effect of compounds on invasion inhibition in cancer cell lines was evaluated. The results indicated that **2f**, **2j**, and quercetin significantly inhibited the invasion of HeLa cells (Figure 8).

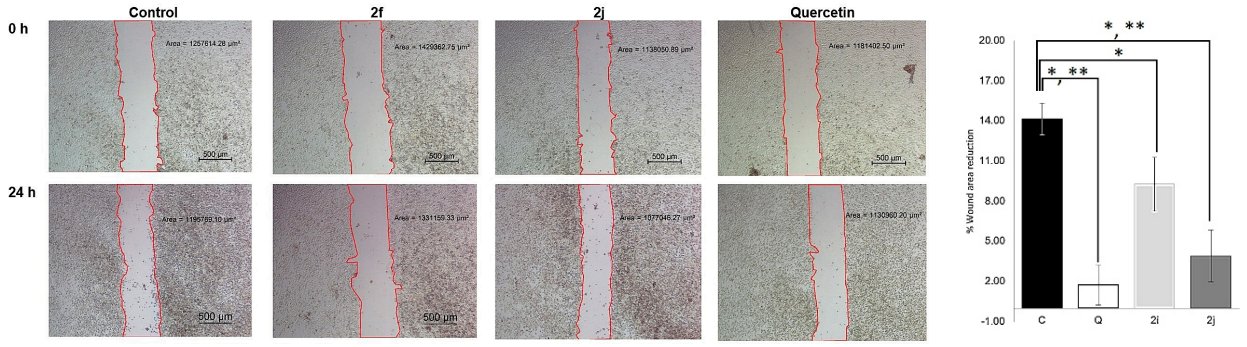


Figure 8. A scratch assay was performed to examine the migration ability of synthesized compounds **2f** and **2j** at 100 µM compared with untreated control. Representative pictures of the assay induce the migration of HeLa cells using quercetin as a reference. Pictures were taken at the start of the experiment (0 h) and 24 h later. Pictures of representative experiments are shown, and the means ± SD are illustrated in the graphs ($n = 3$; *: $p < 0.05$ and **: $p < 0.001$, Turkey HSD). Scale bars represent 500 µm.

3. Materials and Methods

3.1. Apparatus, Chemical and Reagents

Commercially available reagents and solvents were used without further purification. Dry pyridine was drawn under a slightly positive atmosphere of dry nitrogen. The reactions were performed in flame- or oven-dried glassware under a positive dry nitrogen pressure when necessary.

3.2. Synthesis

3.2.1. General Procedure for the Synthesis

In a stirred solution of acetophenone (0.5 g, 1 eq), dry pyridine (10 mL) was slowly added, followed by benzoyl chloride (2.5 eq) and DBU (3 eq). The reaction mixture was refluxed at 120 °C for 24 h, and the pyridine evaporated in vacuo. The mixture was extracted with ethyl acetate (2 × 50 mL). The combined organic layers were washed with water (2 × 50 mL), dried over anhydrous sodium sulfate, and filtered. After evaporation, the crude product was purified by column chromatography.

3.2.2. Characterization of Synthesis Compounds

3-Benzoyl-5-hydroxy-2-phenyl-4H-chromen-4-one (**2a**): Orange solid; 0.746 g of (66.2%); melting point: 156.0–158.0 °C; Rf = 0.553 (hexane: ethyl acetate 7:3); IR 3728.40, 3339, 3063, 2930, 2857, 1678, 1649, 1472, 1229 cm^{-1}; ^{1}H-NMR (600 MHz, DMSO-d_6, 25 °C) δ 12.08 (s, 1H), 8.01 (dd, *J* = 8.3, 1.2 Hz, 2H), 7.78 (t, *J* = 8.4 Hz, 1H), 7.67–7.61 (m, 3H), 7.53–7.44 (m, 5H), 7.25 (dd, *J* = 8.4, 0.7 Hz, 1H), 6.91 (dd, *J* = 8.3, 0.7 Hz, 1H). ^{13}C-NMR (151 MHz, DMSO-d_6, 25 °C) δ 192.69, 181.82, 163.86, 160.23, 156.60, 137.16, 134.79, 133.33, 132.38, 131.53, 129.80, 129.52, 129.38, 128.91, 121.26, 111.89, 110.21, 108.34; MS (ESI) *m*/*z* calculated: 342.0892 found: 343.0965 $(M+H)^+$.

3-Benzoyl-6-hydroxy-2-phenyl-4H-chromen-4-one (**2b**): White solid; 0.210 g of (18.4%); melting point: 201.0–203.5 °C; Rf = 0.34 (hexane: ethyl acetate 7:3); IR 3331, 3063, 1900, 1676, 1468, 1359, 1127, 903 cm^{-1}; ^{1}H-NMR (600 MHz, DMSO-d_6, 25 °C) δ 10.19 (br s, 1H), 7.97–7.85 (m, 2H), 7.70 (dd, *J* = 8.5, 0.9 Hz, 1H), 7.69–7.60 (m, 3H), 7.49–7.43 (m, 5H), 7.34 (m, 2H); ^{13}C-NMR (151 MHz, DMSO-d_6, 25 °C) δ 193.84, 175.94, 162.07, 157.39, 151.14, 137.07, 134.52, 132.05, 131.92, 129.65, 129.45, 129.29, 128.79, 124.57, 123.82, 121.83, 120.88, 107.89; MS (ESI) *m*/*z* calculated: 342.0892 found: 343.0964 $(M+H)^+$.

3-Benzoyl-6-methoxy-2-phenyl-4H-chromen-4-one (**2c**): Yellow solid; 0.159 g of (13.5%); melting point: 194.0–196.0 °C; Rf = 0.683 (hexane: ethyl acetate 7:3); IR 3624, 3071, 2965, 2932, 2835, 1651, 1483, 1368, 1258 cm^{-1}; ^{1}H-NMR (600 MHz, DMSO-d_6, 25 °C) δ 7.92 (d, *J* = 7.3 Hz, 2H), 7.79 (d, *J* = 9.2 Hz, 1H), 7.65–7.58 (m, 3H), 7.52 (dd, *J* = 9.2, 3.1 Hz, 1H), 7.48–7.43 (m, 6H), 3.88 (s, 3H). ^{13}C-NMR (151 MHz, DMSO-d_6, 25 °C) δ 193.84, 175.94, 162.07, 157.39, 151.14, 137.07, 134.52, 132.05, 131.92, 129.65, 129.45, 129.29, 128.79, 124.57, 123.82, 121.83, 120.88, 105.15, 56.32; MS (ESI) *m*/*z* calculated: 356.1049 found: 357.1119 $(M+H)^+$.

3-Benzoyl-7-hydroxy-2-phenyl-4H-chromen-4-one (**2d**): White solid; 0.281 g of (24.8%); melting point: 270.0–271.0 °C; Rf = 0.53 (hexane: ethyl acetate 5:5); IR 3187, 3061, 1671, 1618, 1577, 1506, 1450, 1377, 1241 cm^{-1}; ^{1}H-NMR (600 MHz, DMSO-d_6, 25 °C) δ 7.91 (dd, *J* = 8.4, 5.2 Hz, 3H), 7.63–7.58 (m, 3H), 7.48 (dd, *J* = 9.6, 5.9 Hz, 3H), 7.44 (d, *J* = 7.8 Hz, 2H), 7.02–6.98 (m, 2H); ^{13}C-NMR (151 MHz, DMSO-d_6, 25 °C) δ 193.95, 175.39, 163.90, 161.52, 158.17, 137.14, 134.45, 132.09, 131.78, 129.59, 129.43, 129.26, 128.71, 127.29, 122.17, 116.12, 115.74, 103.08; MS (ESI) *m*/*z* calculated: 342.0892 found: 343.0961 $(M+H)^+$.

3-Benzoyl-5,7-dihydroxy-2-phenyl-4H-chromen-4-one (**2e**): Yellow solid; 0.090 g of (8.2%); melting point: 196.0–197.0 °C; Rf = 0.25 (hexane: ethyl acetate 7:3); IR 3204, 3011, 1628, 1588, 1459, 1369, 1280, 762 cm^{-1}; ^{1}H-NMR (600 MHz, DMSO-d_6, 25 °C) δ 12.23 (s, 1H), 11.11 (s, 1H), 7.94 (d, *J* = 7.9 Hz, 2H), 7.65–7.55 (m, 3H), 7.47–7.41 (m, 5H), 6.53 (s, 1H), 6.28 (s, 1H). ^{13}C-NMR (151 MHz, DMSO-d_6, 25 °C) δ 192.90, 180.30, 165.51, 162.76, 161.91, 158.07, 137.01, 134.69, 132.15, 131.60, 129.71, 129.50, 129.32, 128.78, 120.68, 103.84, 99.89, 94.87; MS (ESI) *m*/*z* calculated: 358.0841 found: 359.0913 $(M+H)^+$.

3-Benzoyl-7,8-dihydroxy-2-phenyl-4H-chromen-4-one (**2f**): Yellow solid; 0.091 g of (7.3%); melting point: 221.5–223.0 °C; Rf = 0.27 (hexane: ethyl acetate 4:6); IR 3112, 3009, 2956, 1652, 1557, 1448, 1368, 1268, cm^{-1}; ^{1}H-NMR (600 MHz, DMSO-d_6, 25 °C) δ 10.54 (s, 1H), 9.57 (s, 1H), 7.89 (dd, *J* = 14.0, 1.2 Hz, 2H), 7.69–7.57 (m, 3H), 7.55–7.38 (m, 6H), 7.02 (d, *J* = 8.7 Hz, 1H). ^{13}C-NMR (151 MHz, DMSO-d_6, 25 °C) δ 194.19, 175.92, 161.34, 151.58, 147.27, 137.21, 134.40, 133.69, 132.19, 131.75, 129.57, 129.43, 129.19, 128.88, 121.59, 116.51, 115.81, 114.99; MS (ESI) *m*/*z* calculated: 358.0841 found: 359.0910 $(M+H)^+$.

7-Hydroxy-3-(3-methoxybenzoyl)-2-(3-methoxyphenyl)-4H-chromen-4-one (**2g**): Yellow solid; yield 38.6%; melting point: 253.0–254.0 °C; Rf = 0.48 (hexane: ethyl acetate 5:5); IR 3046, 2887, 1680, 1627, 1609, 1583, 1459, 1233, cm^{-1}; ^{1}H-NMR (600 MHz, DMSO-d_6, 25 °C) δ 10.97 (s, 1H), 7.96–7.72 (m, 3H), 7.63–7.51 (m, 2H), 7.06–6.90 (m, 5H), 3.82 (s, 3H), 3.76 (s, 3H); ^{13}C-NMR (151 MHz, DMSO-d_6, 25 °C) δ 193.65, 175.39, 163.84, 161.14, 160.02, 159.50, 158.12, 138.56, 133.32, 130.70, 130.58, 127.26, 122.60, 122.24, 120.94, 120.52, 117.35, 116.09, 115.78, 114.23, 113.43, 103.14, 55.86, 55.61; MS (ESI) *m*/*z* calculated: 402.1103 found: 403.1165 $(M+H)^+$.

7-hydroxy-3-(4-methoxybenzoyl)-2-(4-methoxyphenyl)-4H-chromen-4-one (**2h**): Yellow solid; yield 28.0%; melting point: 300.0–301.0 °C; Rf = 0.63 (hexane: ethyl acetate 5:5); IR 3108, 3075, 2957, 1662, 1606, 1506, 1456, 1262, 1029, cm^{-1}; ^{1}H-NMR (600 MHz, DMSO-d_6, 25 °C) δ 11.01 (s, 1H), 7.91 (d, *J* = 8.6 Hz, 1H), 7.52–7.48 (m, 1H), 7.42–7.33 (m, 3H), 7.23–7.19 (m, 1H), 7.19–7.15 (m, 1H), 7.15–7.13 (m, 1H), 7.08–7.04 (m, 1H), 7.03–6.98 (m, 2H), 3.78 (s, 3H), 3.67 (s, 3H); ^{13}C-NMR (151 MHz, DMSO-d_6, 25 °C) δ 192.48, 175.40, 164.19, 163.66, 161.93, 160.74, 158.01, 132.06, 130.39, 130.35, 127.22, 124.24, 121.28, 115.86, 115.71, 114.74, 114.68, 103.00, 56.06, 55.87; MS (ESI) *m*/*z* calculated: 402.1103 found: 403.1166 $(M+H)^+$.

7-hydroxy-3-(4-nitrobenzoyl)-2-(4-nitrophenyl)-4H-chromen-4-one (**2i**): Yellow solid; yield 5.2%; melting point: 290.0–291.0 °C; Rf = 0.54 (hexane: ethyl acetate 5:5); IR 3225, 3108, 1680, 1621, 1524, 1453, 1347, 1238, 1109 cm^{-1}; ^{1}H-NMR (600 MHz, DMSO-d_6, 25 °C) δ 11.26 (s, 1H), 8.31–8.26 (m, 4H), 8.24–8.20 (m, 2H), 7.91 (d, *J* = 8.7 Hz, 1H), 7.88–7.84 (m, 2H), 7.06 (dd, *J* = 15.5, 5.0 Hz, 2H); ^{13}C-NMR (151 MHz, DMSO-d_6, 25 °C) δ 192.48, 175.40, 164.19, 163.66, 161.93, 160.74, 158.01, 132.06, 130.39, 130.35, 127.22, 124.24, 121.28, 115.86, 115.71, 114.74, 114.68, 103.00; MS (ESI) *m*/*z* calculated: 432.0594 found: 433.0651 $(M+H)^+$.

3-Benzoyl-8-hydroxy-4-oxo-2-phenyl-4H-chromen-7-yl benzoate (**2j**): Orange solid; 0.2686 g of (25.0%); melting point: 205.0–206.0 °C; Rf = 0.125 (hexane: ethyl acetate 7:3); IR 3163.26, 1741.72, 1450.47, 1386.84, 1328.95cm^{-1}; ^{1}H-NMR (600 MHz, DMSO-d_6, 25 °C) δ 11.43 (s, 1H), 8.22 (t, *J* = 7.0 Hz, 2H), 7.92 (d, *J* = 8.1 Hz, 2H), 7.87 (d, *J* = 8.9 Hz, 1H), 7.81–7.76 (m, 1H), 7.68–7.60 (m, 3H), 7.51–7.46 (m, 2H), 7.41 (d, *J* = 8.0 Hz, 2H), 7.39–7.34 (m, 1H), 7.27 (t, *J* = 7.8 Hz, 2H), 7.22 (d, *J* = 8.9 Hz, 1H). ^{13}C-NMR (151 MHz, DMSO-d_6, 25 °C) δ 193.65, 175.23, 164.31, 160.91, 155.74, 150.14, 137.01, 134.93, 134.62, 132.04, 131.64, 130.49, 129.62, 129.51, 129.44, 129.28, 128.55, 128.29, 126.24, 123.67, 122.25, 116.22, 116.09; MS (ESI) *m*/*z* calculated: 462.1103 found: 463.1175 $(M+H)^+$.

6-Acetyl-2,3-dihydroxyphenyl benzoate (**3i**): White solid; 0.2251 g of (24.9%); melting point: 166.5–168.0 °C; Rf = 0.52 (hexane: ethyl acetate 5:5); IR 3096, 2930, 1742, 1283, 1260, 1067, 700 cm^{-1}; ^{1}H-NMR (500 MHz, DMSO-d_6, 25 °C) δ 12.81 (s, 1H), 11.04 (s, 1H), 8.12 (d, *J* = 7.2 Hz, 2H), 7.74 (t, *J* = 7.4 Hz, 2H), 7.60 (t, *J* = 7.7 Hz, 2H), 6.58 (d, *J* = 8.9 Hz, 1H), 2.57 (s, 3H). ^{13}C-NMR (151 MHz, DMSO-d_6, 25 °C) δ 204.06, 164.06, 157.06, 156.43, 134.47, 130.57, 130.35, 129.42, 129.11, 126.11, 113.69, 108.37, 26.85; MS (ESI) *m*/*z* calculated: 254.0685 found: 273.0757 $(M+H)^+$.

2-Acetyl-5-hydroxyphenyl furan-2-carboxylate (**4**): White solid; 0.1969 g of (17.5%); melting point: 122.0–124.0 °C; Rf = 0.80 (hexane: ethyl acetate 5:5); IR 3102, 3066, 2990, 1755, 1263, 1045, 704; ^{1}H-NMR (600 MHz, DMSO-d_6, 25 °C) δ 12.20 (s, 1H), 8.13 (dd, *J* = 1.6, 0.7 Hz, 1H), 8.00 (d, *J* = 8.6 Hz, 1H), 7.61 (dd, *J* = 3.6, 0.7 Hz, 1H), 6.97–6.87 (m, 2H), 6.82 (dd, *J* = 3.6, 1.7 Hz, 1H), 2.66 (s, 3H). ^{13}C-NMR (151 MHz, DMSO-d_6, 25 °C) δ 204.04, 162.48, 156.00, 155.81, 149.43, 143.08, 133.44, 121.22, 119.22, 113.66, 113.36, 111.08, 28.27; MS (ESI) *m*/*z* calculated: 246.0528 found: 247.0601 $(M+H)^+$. (Figures S1–S11: ^{1}H-NMR spectrum

of compound **2a**–**3i**; Figure S12: ^{1}H-NMR spectrum of compound **4**; Figures S13–S23: ^{13}C-NMR spectrum of compound **2a**–**3i**; Figure S24: ^{13}C-NMR spectrum of compound **4**; Figures S25–S35: Mass spectrum (MS-ESI) of com-pound **2a**–**3i**; Figure S36: Mass spectrum (MS-ESI) of compound **4**).

3.3. Antioxidant Activity

3.3.1. DPPH Assay

The DPPH method was followed and modified from a previous study [33]. Trolox was used as a reference. The DPPH stock solution at a concentration of 0.625 mM was prepared in 50% ethanol and kept at 4 °C in the dark. On the day of the experiment, 0.208 mM fresh DPPH working solution was freshly prepared by further diluting with 50% ethanol. Trolox and sample stock solutions were prepared in a serial dilution with 50% ethanol at concentrations ranging from 12.5–750 µM and stored at 4 °C. Each reaction was carried out in a 96-well plate, and 100 µL of test preparation and DPPH solution were added. The 96-well plate was then shaken well for 10 min and kept in the dark at room temperature for 20 min, and the absorbance was recorded at 515–517 nm. According to the method described, delocalization also results in a deep violet color and is quantified as a percentage of scavenging activity.

$$\% \text{ scavenging activity (SA)} = 100 \times (A_{sample} - A_{blank})/(A_{control} - A_{blank}) \quad (1)$$

where $A_{control}$ and A_{sample} are the absorbances of the test DPPH without and with a sample, respectively. A_{blank} is the absorbance of the solvent used. The EC_{50} values were calculated from the relationship curve of %SA versus sample concentration. The experiment was carried out at least in triplicate.

3.3.2. FRAP Assay

The FRAP assay is a method for assessing antioxidant power. Briefly, the FRAP reagent was prepared from acetate buffer pH 3.6, 10 mM TPTZ solution in 40 mM HCl and 20 mM $FeCl_3$.6 H_2O in relative proportions of 10:1:1, *v*/*v*, respectively. The FRAP reagent was freshly prepared daily. A solution of 5 µL of the sample (3–300 µM, *approx.*) was mixed with 180 µL of the FRAP reagent in a 96-well plate. The mixture was shaken in the dark for 10 min and incubated at 37 °C for 20 min, and the absorbance was determined at 593 nm. The solution without the sample was used as a blank. All determinations were made in triplicate. Trolox was used as a standard antioxidant and plot the calibration curve between absorbance and concentration. Quercetin was applied as the reference compound. The FRAP values were calculated by comparing the absorbance change in the test sample and represented in µM of Trolox equivalent per µM of sample.

3.3.3. ABTS Assay

The ABTS assay was prepared by reaction of 5 mL of a 7 mM aqueous ABTS (2,2′-azino-bis (3-ethylbenzthiazoline-6-sulphonic acid) solution and 2.45 mM potassium persulfate solution ($K_2S_2O_8$) [34]. After preparation and storage in the dark for 16 h, the radical cation solution was further diluted in ethanol to absorb about 0.7 at 734 nm. Trolox and test sample solutions were prepared in stock solution with DMSO and diluted with ethanol. A solution of 100 µL of the sample was mixed with 100 µL of the ABTS reagent in a 96-well plate. The mixture was shaken in a dark place for 10 min and incubated at 37 °C for 20 min, and the absorbance was determined at 734 nm. Absorbance determinations were recorded immediately and not more than 1 h after adding the reagent. The solution without the sample was used as a blank. All the determinations were made in triplicate. The sample's scavenging percentage was calculated from this equation: scavenging percentage = (Absorbance $_{control}$ − Absorbance $_{sample}$) × 100/Absorbance $_{control}$. EC_{50} values were calculated from the relationship curve of %scavenging versus sample concentration.

3.4. Cell Culture

HEK293, HACAT, and HeLa cells were grown in modified Eagles' minimum essential medium (EMEM, Gibco) with 10% fetal bovine serum (FBS, Gibco), 1% of 100 U/mL streptomycin and 100 U/mL penicillin (Gibco). Cells were seeded in culture flasks and maintained in an incubator at 37 °C in a humidified atmosphere with 5% CO_2. After reaching 80–90% of confluence, cells were detached by incubation with 0.25% trypsin-0.2% EDTA (Gibco) for 5 min and plated for experiments.

3.5. Cytotoxicity Assay

This study examined cell cultures of HEK293, HACAT, and HeLa cells. The cytotoxicity of the test samples was carried out by the MTT (3-(4,5-dimethylthiazol-2-yl)-2,5-diphenyltetrazolium bromide) assay. The cells were seeded in 96-well microliter plates (2.0×10^4 cells/well). Stock solutions of the test compounds were prepared in DMSO. After 24 h, cells were treated with different concentrations of samples and diluted with media to obtain the final desired concentration. The treated cells were then incubated at 37 °C and 5% CO_2 for 24 and 48 h. After incubation, the medium was replaced with 0.05% *w*/*v* of MTT solution in PBS and further incubated for 3 h. The solution was then discarded and DMSO was added to dissolve the formed formazan crystals. Each well's absorbance (A) was measured at 570 nm using a microplate reader (FLUOstar Omega^{TM}, BMG Labtech, Ortenberg, Germany). All experiments were carried out in triplicate and repeated for at least three experiments.

3.6. Cellular ROS Assay

In this study, Hela cells were seeded overnight at 20,000 cells/90 µL/well in a black wall/clear bottom 96-well plate. Cells included those untreated (control) and those pre-treated with compounds at various concentrations (50, 100, 150 µM) for 24 h. The ROS deep red assay solution (100 µL/well) was added and incubated at 5% CO_2, 37 °C incubator for 30 min. The fluorescence signal was monitored at Ex/Em = 650/675 nm (cut off = 665 nm) with bottom read mode within 30 min (cellular ROS assay kit, ab186029, abcam).

3.7. Apoptosis

HeLa cells were seeded overnight at 1×10^5 cells/1.5 mL/well in a 6-well plate. The cells were treated with a sample with IC_{50} concentrations and incubated at 37 °C and 5% CO_2 for 24 h. The cells were lyzed and washed with PBS. The collected cells were diluted with serum-free medium to a suitable volume. The 100 µL of cell suspension was added to 100 µL of Muse^{TM} Annexin V & Dead Cell reagent and incubated for 20 min at room temperature. Cells were analyzed by flow cytometry (Guava Muse Cell Analyzer, Luminex, Austin, TX USA) with Guava suite software 3.4.

3.8. Cell Cycle Analysis

The treatment of HeLa cells and compounds was the same as in the apoptosis protocol. The cells were harvested for 200 µL and centrifuged at 600× *g* for 5 min and washed with PBS. The mixing cells were slowly added 200 µL of ice-cold 70% ethanol and incubated for at least 3 h at −20 °C. Cells were centrifuged and washed with PBS. Finally, cells were stained with 200 µL of Muse® cell cycle reagent and incubated at room temperature for 30 min in the dark. The cell was analyzed by flow cytometry (Guava Muse Cell Analyzer, Luminex, Austin, TX, USA).

3.9. Cell Migration Assay

Cell migration in the HEK293 and the HeLa cell lines was investigated. The assay was conducted to investigate cell maintenance after being damaged. The active samples from in vitro antioxidant activity were examined. Cells were grown in a 24-well plate until 80% confluence and treated with **2f** and **2j** for 24 or 48 h compared to the untreated control. The cells in each well were then scratched to create a wound area across the center

of the plates using a plastic 20 µL pipette tip. Cell images were taken immediately, and the scratch area was measured at 0, 24, and 48 h. During the experiment, the percentage of wound area was tracked as an indirect assessment. Compared to the control, the percentage of empty area change at each time point was quantified with a Nikon eclipse Ts2R inverted microscope.

4. Conclusions

In summary, all compounds were synthesized and screened for antioxidant activity. Four compounds—**2e**, **2f**, **2j,** and **3i**—displayed potent antioxidant activity and were safe for normal cells. In addition, all synthesis compounds were investigated for their anticancer activity in cervical cancer cells. Compounds **2b**, **2d**, **2e**, **2f**, **2g**, **2i**, and **2j** also showed activity against cancer, but **2i** exhibited toxicity in normal cells. The compounds **2f** and **2j** at concentration of 50 and 100 µM are observed to protect cells after treatment with hydrogen peroxide. These two compounds were likely to be lead compounds. From the cytotoxicity test and anti-migration in HeLa, compounds **2f** and **2j** exhibited potential chemopreventive properties. Furthermore, **2f** and **2j** can induce cell cycle arrest in the S phase and induce cell apoptosis in HeLa cells. These results encourage the use of these chromone scaffolds as a promising antioxidant and chemopreventive agent. All authors have read and agreed to the published version of the manuscript.

Supplementary Materials: The following are available online at https://www.mdpi.com/article/10.3390/molecules28073129/s1, Figures S1–S11: ^{1}H-NMR spectrum of compound **2a–3i**; Figure S12: ^{1}H-NMR spectrum of compound **4**; Figures S13–S23: ^{13}C-NMR spectrum of compound **2a–3i**; Figure S24: ^{13}C-NMR spectrum of compound **4**; Figures S25–S35: Mass spectrum (MS-ESI) of compound **2a–3i**; Figure S36: Mass spectrum (MS-ESI) of compound **4**

Author Contributions: Conceptualization, S.T. and C.M.; Methodology, S.T., C.M. and J.U.; Software, S.T.; Formal Analysis, S.T.; Resources, S.T.; Data Curation & structure characterization, C.C., N.P., T.K., K.R. and C.M.; Investigation, K.R. and J.U.; Supervision, S.T.; Writing—Original Draft Preparation, S.T. and C.M; Writing—Review and Editing, S.T. and R.A.; Funding Acquisition, S.T. All authors have read and agreed to the published version of the manuscript.

Funding: This study was supported by Thailand Science Research and Innovation Fundamental Fund (Project ID. TUFF 58/2565) and partially financially supported by the Thammasat University (research project grant TUFT-FF 46/2565) and Thammasat University Research Unit in Drug, Health Product Development and Application (Project ID. 6305001). The authors wish to express their gratitude to faculty of pharmacy, Thammasat University (Thailand) about some equipment for structure characterization.

Institutional Review Board Statement: Not applicable.

Informed Consent Statement: Not applicable.

Data Availability Statement: Not applicable.

Conflicts of Interest: The authors declare no conflict of interest.

Sample Availability: Samples of the compounds are not available from the authors.

References

1. Finkel, T.; Holbrook, N.J. Oxidants, oxidative stress and the biology of ageing. *Nature* **2000**, *408*, 239–247. [CrossRef] [PubMed]
2. Aminjan, H.H.; Abtahi, S.R.; Hazrati, E.; Chamanara, M.; Jalili, M.; Paknejad, B. Targeting of oxidative stress and inflammation through ROS/NF-kappaB pathway in phosphine-induced hepatotoxicity mitigation. *Life Sci.* **2019**, *232*, 116607. [CrossRef] [PubMed]
3. Cadet, J.; Davies, K.J.A.; Medeiros, M.H.G.; Mascio, P.D.; Wagner, J.R. Formation and repair of oxidatively generated damage in cellular DNA. *Free Radic. Biol. Med.* **2017**, *107*, 13–34. [CrossRef] [PubMed]
4. Finkel, T. Oxidant signals and oxidative stress. *Curr. Opin. Cell Biol.* **2003**, *15*, 247–254. [CrossRef]

5. Kurutas, E.B. The importance of antioxidants which play the role in cellular response against oxidative/nitrosative stress: Current state. *Nutr. J.* **2016**, *15*, 71. [CrossRef]
6. Kaminski, K.A.; Bonda, T.A.; Korecki, J.; Musial, W.J. Oxidative stress and neutrophil activation—The two keystones of ischemia/reperfusion injury. *Int. J. Cardiol.* **2002**, *86*, 41–59. [CrossRef] [PubMed]
7. Liang, X.; Wang, S.; Wang, L.; Ceylan, A.F.; Ren, J.; Zhang, Y. Mitophagy inhibitor liensinine suppresses doxorubicin-induced cardiotoxicity through inhibition of drp1-mediated maladaptive mitochondrial fission. *Pharmacol. Res.* **2020**, *157*, 104846. [CrossRef]
8. López-Otín, C.; Galluzzi, L.; Freije, J.M.; Madeo, F.; Kroemer, G. Metabolic control of longevity. *Cell* **2016**, *166*, 802–821. [CrossRef]
9. Liguori, I.; Russo, G.; Aran, L.; Bulli, G.; Curcio, F.; Della-Morte, D.; Gargiulo, G.; Testa, G.; Cacciatore, F.; Bonaduce, D.; et al. Sarcopenia: Assessment of disease burden and strategies to improve outcomes. *Clin. Interv. Aging* **2018**, *13*, 913–927. [CrossRef]
10. Sackesen, C.; Ercan, H.; Dizdar, E.; Soyer, O.; Gumus, P.; Tosun, B.N.; Büyüktuncer, Z.; Karabulut, E.; Besler, T.; Kalayci, O. A comprehensive evaluation of the enzymatic and nonenzymatic antioxidant systems in childhood asthma. *J. Allergy Clin. Immunol.* **2008**, *122*, 78–85. [CrossRef]
11. Reuter, S.; Gupta, S.C.; Chaturvedi, M.M.; Aggarwal, B.B. Oxidative stress, inflammation, and cancer: How are they linked? *Free Radic. Biol. Med.* **2010**, *49*, 1603–1616. [CrossRef] [PubMed]
12. Birben, E.; Sahiner, U.M.; Sackesen, C.; Erzurum, S.; Kalayci, O. Oxidative stress and antioxidant defense. *World Allergy Organ. J.* **2012**, *5*, 9–19. [CrossRef] [PubMed]
13. Salehi, B.; Martorell, M.; Arbiser, J.L.; Sureda, A.; Martins, N.; Maurya, P.K.; Sharifi-Rad, M.; Kumar, P.; Sharifi-Rad, J. Antioxidants: Positive or negative actors? *Biomolecules* **2018**, *8*, 124. [CrossRef] [PubMed]
14. Tokarz, P.; Blasiak, J. Role of mitochondria in carcinogenesis. *Acta Biochim. Pol.* **2014**, *61*, 671–678. [CrossRef] [PubMed]
15. Zou, Z.; Chang, H.; Li, H.; Wang, S. Induction of reactive oxygen species: An emerging approach for cancer therapy. *Apoptosis* **2017**, *22*, 1321–1335. [CrossRef] [PubMed]
16. Cui, K.; Luo, X.; Murthy, M.R.V. Role of oxidative stress in neurodegeneration: Recent developments in assay methods for oxidative stress and nutraceutical antioxidants. *Prog. Neuropsychopharmacol. Biol. Psych.* **2004**, *28*, 771–799. [CrossRef] [PubMed]
17. Panche, A.N.; Diwan, A.D.; Chandra, S.R. Flavonoids: An overview. *J. Nutr. Sci.* **2016**, *5*, e47. [CrossRef]
18. Wenying, R.; Zhenhua, Q.; Hongwei, W.; Lei, Z.; Li, Z. Flavonoids: Promising anticancer agents. *Med. Res. Rev.* **2003**, *23*, 519–534.
19. Sharifi, R.J.; Hoseini-Alfatemi, S.M.; Sharifi-Rad, M.; Teixeira da Silva, J.A. Antibacterial, antioxidant, antifungal and anti-inflammatory activities of crude extract from Nitraria schoberi fruits. *Biotech* **2015**, *5*, 677–684. [CrossRef]
20. Mead, J.R.; McNair, N. Antiparasitic activity of flavonoids and isoflavones against Cryptosporidium parvum and Encephalitozoon intestinalis. *FEMS Microbiol. Lett.* **2006**, *259*, 153–157. [CrossRef]
21. Wang, T.Y.; Li, Q.; Bi, K.S. Bioactive flavonoids in medicinal plants: Structure, activity and biological fate. *Asian J. Pharm Sci.* **2018**, *13*, 12–23. [CrossRef] [PubMed]
22. Silva, C.F.M.; Batista, V.F.; Pinto, D.; Silva, A.M.S. Challenges with chromone as a privileged scaffold in drug discovery. *Expert Opin. Drug Discov.* **2018**, *13*, 795–798. [CrossRef] [PubMed]
23. Srivastava, S.; Somasagara, R.; Hegde, M.; Nishana, M.; Tadi, S.K.; Srivastava, M.; Choudhary, B.; Raghavan, S.C. Quercetin, a Natural Flavonoid Interacts with DNA, Arrests Cell Cycle and Causes Tumor Regression by Activating Mitochondrial Pathway of Apoptosis. *Sci. Rep.* **2016**, *6*, 24049. [CrossRef] [PubMed]
24. Ganguly, A.K.; Kaur, S.; Mahata, P.K.; Biswas, D.; Pramanik, B.N.; Chan, T.M. Synthesis and properties of 3-acyl-γ-pyrones, a novel class of flavones and chromones. *Tetrahedron. Lett.* **2005**, *46*, 4119–4121. [CrossRef]
25. Maicheen, C.; Jittikoon, J.; Vajragupta, O.; Ungwitayatorn, J. Synthesis, topoisomerase I inhibitory and cytotoxic activities of chromone derivatives. *Med. Chem.* **2013**, *9*, 329–339. [CrossRef]
26. Riva, C.D.; Toma, C.; Donadd, L.; Boi, C.; Pennini, R.; Motta, G.; Leonardi, A. New DBU (1,8-diazabicyclo [5.4.0]undec-7-ene) assisted one-pot synthesis of 2,8-disubstituted 4H-1-benzopyran-4-ones. *Synthesis* **1997**, *2*, 195–201. [CrossRef]
27. Benzie, I.F.; Strain, J.J. The ferric reducing ability of plasma (FRAP) as a measure of antioxidant power: The FRAP assay. *Anal. Biochem.* **1996**, *239*, 70–76. [CrossRef]
28. Rubio, C.P.; Hernández-Ruiz, J.; Martinez-Subiela, S.; Tvarijonaviciute, A.; Ceron, J.J. Spectrophotometric assays for total antioxidant capacity (TAC) in dog serum: An update. *BMC Vet. Res.* **2016**, *12*, 166. [CrossRef]
29. Halliwell, B.; Gutteridge, J.M.C. *Free Radicals in Biology and Medicine*, 4th ed.; Clarendon Press: Oxford, UK, 2006.
30. Tirzitis, G.; Bartosz, G. Determination of antiradical and antioxidant activity: Basic principles and new insights. *Acta Biochim. Pol.* **2010**, *57*, 139–142. [CrossRef]
31. Nenadis, N.; Wang, L.F.; Tsimidou, M.; Zhang, H.Y. Estimation of Scavenging Activity of Phenolic Compounds Using the ABTS$^{\bullet+}$ Assay. *J. Agric. Food Chem.* **2004**, *52*, 4669–4674. [CrossRef]
32. Vidya Priyadarsini, R.; Senthil Murugan, R.; Maitreyi, S.; Ramalingam, K.; Karunagaran, D.; Nagini, S. The flavonoid quercetin induces cell cycle arrest and mitochondria-mediated apoptosis in human cervical cancer (HeLa) cells through p53 induction and NF-κB inhibition. *Eur. J. Pharmacol.* **2010**, *649*, 84–91. [CrossRef] [PubMed]

33. Cheng, Z.; Moore, J.; Yu, L. High-Throughput Relative DPPH Radical Scavenging Capacity Assay. *J. Agric. Food Chem.* **2006**, *54*, 7429–7436. [CrossRef] [PubMed]
34. Re, P.; Pellegrini, N.; Proteggente, A.; Pannala, A.; Yang, M.; Rice-Evans, C. Antioxidant activity applying an improved ABTS radical cation decolorization assay. *Free Radic. Biol. Med.* **1999**, *26*, 1231–1237. [CrossRef] [PubMed]

Disclaimer/Publisher's Note: The statements, opinions and data contained in all publications are solely those of the individual author(s) and contributor(s) and not of MDPI and/or the editor(s). MDPI and/or the editor(s) disclaim responsibility for any injury to people or property resulting from any ideas, methods, instructions or products referred to in the content.